Artificial Intelligence in Medicine 51 (2011) 199–209

Contents lists available at ScienceDirect

Artificial Intelligence in Medicine

journal homepage: www.elsevier.com/locate/aiim

An automated diagnostic system of polycystic ovary syndrome based on object growing

Yinhui Deng[a,1], Yuanyuan Wang[a,*], Yuzhong Shen[b,2]

[a] Department of Electronic Engineering, Fudan University, Shanghai 200433, China
[b] Department of Electrical and Computer Engineering, Old Dominion University, Norfolk, VA 23529, USA

ARTICLE INFO

Article history:
Received 2 March 2009
Received in revised form 15 July 2010
Accepted 8 October 2010

Keywords:
Object growing
Automated detection of follicles
Polycystic ovary syndrome
Ultrasound images

ABSTRACT

Objective: Polycystic ovary syndrome (PCOS) is a complex endocrine disorder that seriously affects women's health. The disorder is characterized by the formation of many follicles in the ovary. Currently the predominant diagnosis is to manually count the number of follicles, which may lead to inter-observer and intra-observer variability and low efficiency. A computer-aided PCOS diagnostic system may overcome these problems. However the methods reported in recently published literature are not very effective and often need human interaction. To overcome these problems, we propose an automated PCOS diagnostic system based on ultrasound images.
Methods and materials: The proposed system consists of two major functional blocks: preprocessing phase and follicle identification based on object growing. In the preprocessing phase, speckle noise in the input image is removed by an adaptive morphological filter, then contours of objects are extracted using an enhanced labeled watershed algorithm, and finally the region of interest is automatically selected. The object growing algorithm for follicle identification first computes a cost map to distinguish between the ovary and its external region and assigns each object a cost function based on the cost map. The object growing algorithm initially selects several objects that are likely to be follicles with very high probabilities and dynamically update the set of possible follicles based on their cost functions. The proposed method was applied to 31 real PCOS ultrasound images obtained from patients and its performance was compared with those of three other methods, including level set method, boundary vector field (BVF) method and the fuzzy support vector machine (FSVM) classifier.
Results: Based on the judgment of subject matter experts, the proposed diagnostic system achieved 89.4% recognition rate (RR) and 7.45% misidentification rate (MR) while the RR and MR of the level set method, the BVF method and the FSVM classifier are around 65.3% and 2.11%, 76.1% and 4.53%, and 84.0% and 16.3%, respectively. The proposed diagnostic system also achieved better performance than those reported in recently published literature.
Conclusion: The paper proposed an automated diagnostic system for the PCOS using ultrasound images, which consists of two major functional blocks: preprocessing phase and follicle identification based on object growing. Experimental results showed that the proposed system is very effective in follicle identification for PCOS diagnosis.

1. Introduction

Polycystic ovary syndrome (PCOS), also known as Stein–Leventhal syndrome or functional ovarian hyperandrogenism, is a complex endocrine disorder associated with a long-term lack of ovulation and excessive androgens [1]. The disorder is characterized by the formation of many follicles in the ovary, a process related to the ovary's failure to release an ovum [1]. PCOS is one of the most common causes of infertility. Symptoms may include various menstrual problems, hirsutism, endocrine abnormalities, acne, obesity, infertility, and diabetes with insulin resistance or hyperinsulinemia. Even if it may not cause an immediate problem, PCOS can have significant long-term effects, including diabetes, heart disease, and endometrial or breast cancer [2]. Accurate early diagnosis of PCOS is very important for its treatment.

Currently the prevalent method used by doctors for the PCOS diagnosis is to manually identify follicles and count the number in ovary ultrasound images, which is then used as a critical criterion

* Corresponding author. Tel.: +86 21 65642756; fax: +86 21 65643526.
E-mail addresses: yinhuideng@gmail.com (Y. Deng), yywang@fudan.edu.cn (Y. Wang).
[1] Tel.: +86 21 55664473.
[2] Tel.: +1 757 683 6366.

0933-3657/$ – see front matter © 2010 Elsevier B.V. All rights reserved.
doi:10.1016/j.artmed.2010.10.002

to determine the PCOS diagnosis. However, manually identifying follicles may cause several problems, such as inter-observer and intra-observer variability and low efficiency. The tedious and time-consuming nature of manual operations for doctors may cause the inaccuracy of the PCOS diagnosis, which could seriously affect the women's health. These problems can be overcome by an intelligent PCOS diagnostic system which automatically identifies follicles and then counts the number of follicles. Nonetheless, to automatically detect follicles in ovary ultrasound images is not an easy task and several issues must be addressed in order to develop an automated PCOS diagnosis system.

Speckle noise is the major source of contamination in ultrasound images [3], which is characterized by a granular pattern of abrupt change of pixel intensity [4]. The extensive presence of speckle noise in ultrasound images makes it difficult to segment the image into different regions, which is critical in automatic follicle detection. In addition, different structures in ovary ultrasound images are not totally distinct and as a result the boundaries between them are neither clear nor continuous. Only a few approaches were proposed before for ovarian follicle analysis using computer-aided methods. Muzzolini et al. segmented one follicle in ultrasound images using multi-resolution textures [5]. Pierson et al. analyzed the responses of the ovary and individual follicles to different medicine stimuli by manually tracing follicular boundaries [6]. Sarty et al. developed a semi-automated method for follicle segmentation, where manual tracing was often required [7]. Krivanek and Sonka segmented the follicle using the watershed segmentation technique [8]. These methods mainly focused on the segmentation of one single follicle. They also required relatively high quality ovary ultrasound images and involved manual operations.

Potočnik and Zazula proposed an automated ovarian follicle segmentation method [9], which first extracted candidates of follicles by region growing and then identified follicles according to four empirical criteria. This method's recognition rate (RR) was reported as around 88% [9]. Although this method was completely automatic, it relied on parameters that were determined empirically. Potočnik and Zazula later improved their method [10,11] and developed several approaches to estimate parameters used for region growing and introduced a sequence of images to identify follicles based on a Kalman filter. Although the new method was more automated or computerized than their previous one, its recognition rate reduced to around 78%. Cigale and Zazula developed an approach for automatic ovarian follicle segmentation based on cellular neural networks [12]. Although this approach had lower computational complexity than previous methods, its recognition rate was merely 60%.

The major difficulty of automated follicle segmentation in ovary ultrasound images is to exactly identify real follicles under the interference of heavy speckle noise in ultrasound images. Various segmentation methods have been developed to extract the contours of objects in ultrasound medical images [13–15]. These segmentation methods were mainly based on boundary or region energy minimization. A straightforward attempt for follicle detection would be to extract the ovary boundary first using these segmentation methods [13–15]. However, the ovary boundaries in ultrasound images usually are not salient and follicles also appear as local minima, making these segmentation methods unsuitable for the purpose of follicle detection. Since follicles may appear as different features in ovary ultrasound images, another attempt for follicle detection would be to design a classifier [16,17] based on these features. However, our experimental results showed that a single follicle is not clearly discriminable from other local minima based on these features. These classification based methods did not take into account the characteristics of the ovary region and the connectivity or neighborhood between follicles. To achieve better results for follicle identification, it is needed to have a method that simultaneously considers the properties of follicles, the boundary information of the ovary and the different region information in the ovary ultrasound image.

In this paper we propose a novel, effective and automated method for the computer-aided diagnosis of PCOS using ovary ultrasound images. The proposed method is based on the fact that follicles always appear as low-echo local minimum areas inside the contour of the ovary. It consists of two major functional blocks: preprocessing phase and follicle identification based on object growing. The preprocessing phase automatically selects the region of interest and extracts the local minima as possible follicle candidates. Then a cost map is computed to distinguish between the ovary and its external region and each object (local minimum) is assigned a cost function based on the cost map. The object growing algorithm initially selects several objects that are likely to be follicles with very high probabilities and dynamically update the set of possible follicles based on their cost functions. The proposed method was applied to 31 ultrasound images obtained from PCOS patients and its results were compared with those of three other methods, including level set, boundary vector field (BVF), and fuzzy support vector machine (FSVM) classifier. Experimental results showed that the proposed method is very effective in follicle identification and achieved better performance than previously proposed ones.

The remainder of this paper is organized as follows. Section 2 describes in detail the proposed method, including the preprocessing phase and follicle identification based on object growing. Section 3 discusses the experimental results of the proposed method and compares its performance with those of three other methods. Some discussions are presented in Section 4 and finally conclusions are drawn in Section 5.

2. Methods

The proposed method consists of two major functional blocks: preprocessing phase and follicle identification based on object growing. The block diagram of the proposed method is shown in Fig. 1.

2.1. Preprocessing phase

The preprocessing phase performs three tasks: adaptive morphological filtering, local minimum extraction, and region of interest selection. First, the speckle noise in the input PCOS ultrasound image is reduced significantly using an adaptive morphological filter we developed recently [18]. Then an enhanced labeled watershed algorithm is proposed to extract local minima that are possible candidates for follicles. Finally the region of interest is computed iteratively based on the spectral residual approach [19]. The results of the preprocessing phase are then used by subsequent object growing for automatic follicle identification.

2.1.1. Adaptive morphological filtering

Speckle noise is characterized by a granular pattern of abrupt changes of pixel values [4] and it is the major source of contamination in ultrasound images [3]. Speckle noise reduces the contrast and obscures diagnostically important details. Various methods have been proposed to suppress speckle noise [20–22]. Among them, the adaptive morphological filter developed by the authors is an effective method for speckle reduction [18], which effectively depresses abrupt changes of pixel values due to the speckle [4] and facilitates subsequent image processing tasks such as segmentation. In this paper, the adaptive morphological filter is used to suppress speckle noise for extraction

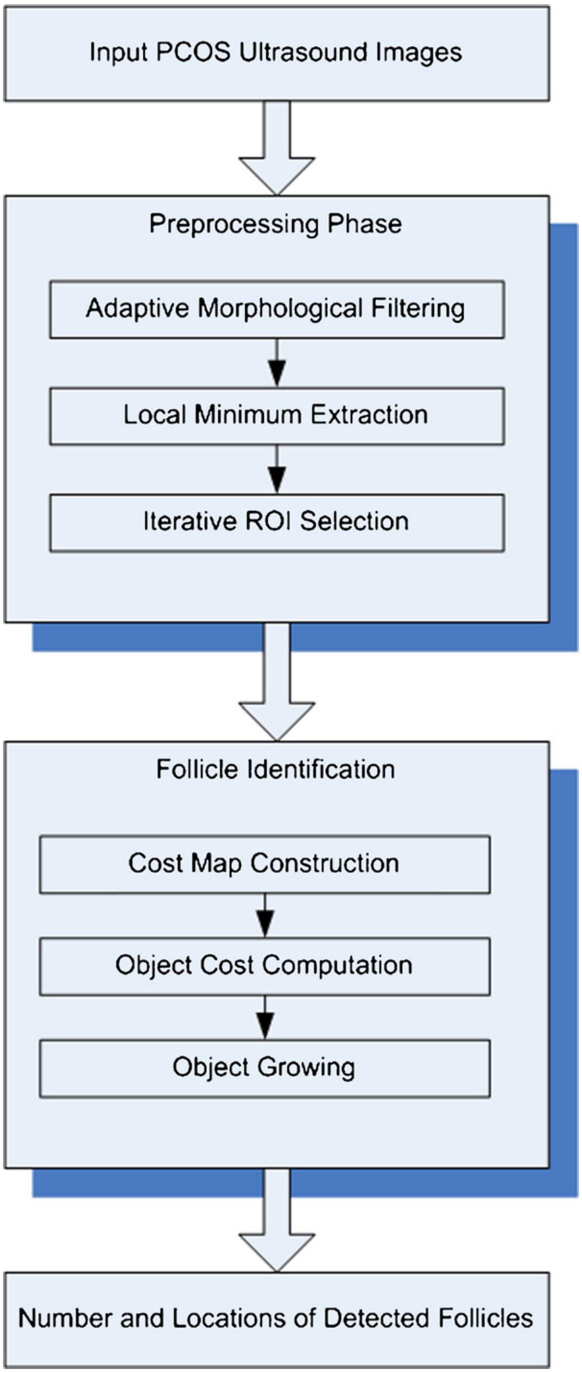

Fig. 1. The block diagram of the proposed automated PCOS diagnostic system.

of local minima. It first computes a set of structuring factors and then constructs the corresponding structuring elements. The structuring factors are used to detect the noise structures in the input image and the structuring elements are applied to effectively suppress the noise based on detected noise structures.

2.1.1.1. Structuring factors. Abrupt changes of pixel values due to the speckle noise mainly appear as "convex" or "concave" structures in one dimension. Thus, we can design a set of structuring factors to represent these noise structures. Assume that the length of abrupt changes due to the speckle noise is less than $2n+1$ pixels. First, a set of row vectors $\boldsymbol{X}$ is defined as

$$\boldsymbol{X} = \begin{bmatrix} \boldsymbol{X}_1 \\ \boldsymbol{X}_2 \\ \vdots \\ \boldsymbol{X}_n \end{bmatrix} = \begin{bmatrix} x_{11} & x_{12} & \cdots & x_{1(2n+1)} \\ x_{21} & x_{22} & \cdots & x_{2(2n+1)} \\ \vdots & \vdots & \ddots & \vdots \\ x_{n1} & x_{n2} & \cdots & x_{n(2n+1)} \end{bmatrix}, \tag{1}$$

where the ith row vector is $\boldsymbol{X}_i = [x_{i1}, \; x_{i2}, \; \ldots, \; x_{i(2n+1)}]$, $x_{ij} = \begin{cases} -1 & \text{when } |j-n-1| < i \\ 1 & \text{else} \end{cases}$. For example, $\boldsymbol{X} = \begin{bmatrix} 1 & 1 & -1 & 1 & 1 \\ 1 & -1 & -1 & -1 & 1 \end{bmatrix}$ when $n=2$ and $\boldsymbol{X} = \begin{bmatrix} 1 & 1 & 1 & -1 & 1 & 1 & 1 \\ 1 & 1 & -1 & -1 & -1 & 1 & 1 \\ 1 & -1 & -1 & -1 & -1 & -1 & 1 \end{bmatrix}$ when $n=3$. $\boldsymbol{X}'_i$ can be further computed by normalizing $\boldsymbol{X}_i$ after subtracting the mean value of $\boldsymbol{X}_i$. The resulting set of row vectors is denoted as $\boldsymbol{W}$,

$$\boldsymbol{W} = \begin{bmatrix} \boldsymbol{X}'_1 \\ \boldsymbol{X}'_2 \\ \vdots \\ \boldsymbol{X}'_n \end{bmatrix} = \begin{bmatrix} \boldsymbol{W}_1 \\ \boldsymbol{W}_2 \\ \vdots \\ \boldsymbol{W}_n \end{bmatrix} = \begin{bmatrix} w_{11} & w_{12} & \cdots & w_{1(2n+1)} \\ w_{21} & w_{22} & \cdots & w_{2(2n+1)} \\ \vdots & \vdots & \ddots & \vdots \\ w_{n1} & w_{n2} & \cdots & w_{n(2n+1)} \end{bmatrix}. \tag{2}$$

Each row vector can represent the specific "concave" structure in one dimension and is used to detect abrupt changes of different length.

To detect features of different directions, a set of new structuring factors $\boldsymbol{W}_{i1}, \boldsymbol{W}_{i2}, \boldsymbol{W}_{i3}, \boldsymbol{W}_{i4}$ are constructed based on $\boldsymbol{W}_i$ as

$$\begin{aligned} \boldsymbol{W}_{i1} &= \begin{bmatrix} w_{i1} & w_{i2} & \cdots & w_{i(2n+1)} \end{bmatrix}, \\ \boldsymbol{W}_{i2} &= \begin{bmatrix} w_{i1} & & & \\ & w_{i2} & & \\ & & \ddots & \\ & & & w_{i(2n+1)} \end{bmatrix}, \\ \boldsymbol{W}_{i3} &= \begin{bmatrix} w_{i1} \\ w_{i2} \\ \vdots \\ w_{i(2n+1)} \end{bmatrix}, \\ \boldsymbol{W}_{i4} &= \begin{bmatrix} & & & w_{i1} \\ & & w_{i2} & \\ & \iddots & & \\ w_{i(2n+1)} & & & \end{bmatrix}. \end{aligned} \tag{3}$$

To represent all possible noise structures, we need an array of size $n \times 4$, that is, $\begin{bmatrix} \boldsymbol{W}_{11} & \boldsymbol{W}_{12} & \boldsymbol{W}_{13} & \boldsymbol{W}_{14} \\ \boldsymbol{W}_{21} & \boldsymbol{W}_{22} & \boldsymbol{W}_{23} & \boldsymbol{W}_{24} \\ \vdots & \vdots & \vdots & \vdots \\ \boldsymbol{W}_{n1} & \boldsymbol{W}_{n2} & \boldsymbol{W}_{n3} & \boldsymbol{W}_{n4} \end{bmatrix}$. Elements in this array can represent different structures of abrupt changes of pixel values. In the following section, we will discuss how to construct corresponding structuring elements for morphological filtering based on the detected speckle noise structures.

2.1.1.2. Structuring elements. Opening and closing operations are commonly used morphological operations [23]. The morphological opening can depress "convex" structures whose size is smaller than the structuring element while the morphological closing can depress "concave" structures whose size is smaller than the structuring element. In order to perform adaptive morphological filtering based on different noise structures, we define the following structuring elements $\boldsymbol{B}_{i1}, \boldsymbol{B}_{i2}, \boldsymbol{B}_{i3}, \boldsymbol{B}_{i4}$ for the structuring factors $\boldsymbol{W}_{i1}, \boldsymbol{W}_{i2}, \boldsymbol{W}_{i3}, \boldsymbol{W}_{i4}$ defined in the previous section.

$$\boldsymbol{B}_{i1} = \underbrace{\begin{bmatrix} 1 & 1 & \cdots & 1 \end{bmatrix}}_{(i+1)},$$
$$\boldsymbol{B}_{i2} = \underbrace{\begin{bmatrix} 1 & & & \\ & 1 & & \\ & & \ddots & \\ & & & 1 \end{bmatrix}}_{(i+1)},$$
$$\boldsymbol{B}_{i3} = \left.\begin{bmatrix} 1 \\ 1 \\ \vdots \\ 1 \end{bmatrix}\right\} (i+1),$$
$$\boldsymbol{B}_{i4} = \underbrace{\begin{bmatrix} & & & 1 \\ & & 1 & \\ & \iddots & & \\ 1 & & & \end{bmatrix}}_{(i+1)}. \tag{4}$$

Such structuring elements enable the precise depression of specific abrupt changes of pixel values due to the speckle. Morphological operation with different structuring elements will be applied to different regions based on the detected speckle noise structure in that region.

2.1.1.3. Morphological filtering. To detect the noise structures, the original ultrasound image $\boldsymbol{I}_{orig}$ is convolved with each structuring factor as follows

$$\boldsymbol{I}_{ij}^{SF} = \boldsymbol{I}_{orig} \otimes \boldsymbol{W}_{ij} \quad i = 1\text{–}n, \quad j = 1\text{–}4 \tag{5}$$

where $\otimes$ represents the operation of convolution and $\boldsymbol{I}_{ij}^{SF}$ is the result of convolution of $\boldsymbol{I}_{orig}$ with structuring factor $\boldsymbol{W}_{ij}$. Thus a total of $n \times 4$ images are obtained after this convolution; in other words, there are $n \times 4$ resulting values for each pixel location (p, q) as shown below.

$$\begin{bmatrix} \boldsymbol{I}_{11}^{SF}(p,q) & \boldsymbol{I}_{12}^{SF}(p,q) & \boldsymbol{I}_{13}^{SF}(p,q) & \boldsymbol{I}_{14}^{SF}(p,q) \\ \boldsymbol{I}_{21}^{SF}(p,q) & \boldsymbol{I}_{22}^{SF}(p,q) & \boldsymbol{I}_{23}^{SF}(p,q) & \boldsymbol{I}_{24}^{SF}(p,q) \\ \vdots & \vdots & \vdots & \vdots \\ \boldsymbol{I}_{n1}^{SF}(p,q) & \boldsymbol{I}_{n2}^{SF}(p,q) & \boldsymbol{I}_{n3}^{SF}(p,q) & \boldsymbol{I}_{n4}^{SF}(p,q) \end{bmatrix}$$

In the above matrix, the element with the largest norm, denoted as $\boldsymbol{I}_{MN}^{SF}(p,q)$, represents the most possible structure of abrupt changes in the pixel's neighborhood. Then the corresponding structuring element $\boldsymbol{B}_{MN}$ defined in Eq. (4) is used to perform morphological filtering of $\boldsymbol{B}_{orig}$ in the neighborhood determined by the structuring element $\boldsymbol{B}_{MN}$. If the value $\boldsymbol{I}_{MN}^{SF}(p,q)$ is positive, a closing operation is applied; otherwise, an opening operation is applied. The resulting image after adaptive morphological filtering is denoted as $\boldsymbol{I}_{despeckled}$.

2.1.2. Local minimum extraction

After adaptive morphological filtering, it is necessary to extract local minima where follicles can possibly appear. The watershed algorithm is an effective segmentation method to detect multiple objects [24]. However, the classical watershed algorithm often leads to excessive segmentations, especially for noisy images such as ultrasound images. The labeled watershed algorithm was developed to overcome this problem [23] and it introduced a label mask to locate primary local minima. With the label mask, secondary local minima are depressed. However, the computation of the label mask is dependent on a threshold parameter indicating whether the local minimum is primary or secondary according to its depth [23]. The threshold parameter is often empirically determined. In addition, primary local minima may have significantly varying depths, often leading to omissions of primary local minima due to the use of only one single threshold value. In this paper, we propose an enhanced labeled watershed algorithm that utilizes a more robust method to compute the label mask. The enhanced labeled watershed algorithm is detailed as follows.

First, the edges in the denoised image $\boldsymbol{I}_{despeckled}$ are computed using Sobel edge detection [23] and the resulting image is denoted as $\boldsymbol{I}_{edge}$. Then a gray depth image $\boldsymbol{I}_{depth}$ is computed based on $\boldsymbol{I}_{despeckled}$ as follows,

$$\boldsymbol{I}_{depth} = 1 - \frac{1}{T}\int_0^T \boldsymbol{M}(\boldsymbol{I}_{despeckled}, x)dx, \tag{6}$$

where T is a parameter defining the upper limit of gray depth in an image, $\boldsymbol{M}(\boldsymbol{I}, x)$ is a masking function that finds pixels in the area of local minima of image $\boldsymbol{I}$ whose gray depth is greater than x [23]. $\boldsymbol{M}(\boldsymbol{I}, x)$ is defined as

$$\boldsymbol{M}(\boldsymbol{I}, x) = \begin{cases} 1 & \text{for pixels in the area of local minima of} \\ & \quad I \text{ whose gray depth is greater than } x \\ 0 & \text{else} \end{cases} \tag{7}$$

For a discrete image whose gray range is from 0 to 255, Eq. (6) can be rewritten as

$$\boldsymbol{I}_{depth} = 1 - \frac{1}{255}\sum_{x=0}^{255} \boldsymbol{M}(\boldsymbol{I}_{despeckled}, x) \tag{8}$$

The gray depth image $\boldsymbol{I}_{depth}$ describes the gray depth property of an image based on its local minima. Each primary local minimum in the image $\boldsymbol{I}_{despeckled}$ is transformed into a more uniform local minimum in its gray depth image $\boldsymbol{I}_{depth}$ using Eqs. (6) and (7).

A series of operations is then applied to the gray depth image $\boldsymbol{I}_{depth}$ in order to compute the watershed boundary. First a morphological closing operation with a structuring element of size 3×3 is applied to $\boldsymbol{I}_{depth}$ to suppress noise and the resulting image is denoted as $\boldsymbol{I}_{depth\_smooth}$, which is then used as the input to the function $\boldsymbol{M}(\boldsymbol{I}_{depth\_smooth}, x)$ with x set to 1. The resulting image, denoted as $\boldsymbol{I}_{min\_mask}$, represents the primary local minima of the original image $\boldsymbol{I}_{orig}$. An Euclidean distance transform is then applied to $\boldsymbol{I}_{min\_mask}$ to generate the image $\boldsymbol{I}_{min\_dist}$. Both $\boldsymbol{I}_{min\_mask}$ and the watershed boundary of $\boldsymbol{I}_{min\_dist}$ are used as the label mask. The edge pixels in the pixel map $\boldsymbol{I}_{edge}$ located in the label mask are then set to the minimum of $\boldsymbol{I}_{edge}$ within the mask; the watershed boundary of the resulting image is computed and is denoted as $\boldsymbol{I}_{bound\_watershed}$. The extracted watershed boundaries are contours of objects and some of them contain follicles. The next step is to select a region of interest to reduce the image size and thus the number of local minima that are possibly follicles.

2.1.3. Iterative region of interest selection

Selecting an appropriate region of interest (ROI) can reduce computational complexity and improve accuracy in computer vision and pattern recognition. Among the various methods proposed for ROI selection [19,25,26], the spectral residual approach [19] is an effective approach that is independent of features, object categories, or other forms of prior knowledge of objects. By analyzing the log-spectrum of an input image, the spectral residual approach extracts the spectral residual of an image in the spectral domain, which contains the saliency information of the image [19]. Then the corresponding saliency map is constructed in the spatial domain by applying exponential transform, inverse Fourier transform, and Gaussian filtering to the spectral residual. The larger gray values in the saliency map represent more saliency at the corresponding locations.

To improve the performance of the spectral residual approach, in this paper we propose an iterative ROI selection algorithm based on the spectral residual approach. The essence of the spectral residual approach is to find the region with more variations in the spectral domain. To take advantage of the polycystic characteristic of the ovary in the ultrasound image, the result of the enhanced labeled watershed algorithm, $\boldsymbol{I}_{bound\_watershed}$, is used as the input image of the proposed iterative ROI selection algorithm, which is detailed as follows.

(a) Calculate the saliency map of the input image with the spectral residual approach.
(b) Locate the pixel with the largest value in the saliency map. Resize the input image with this pixel as the center with a new size calculated as $1-\sum_{k=1}^{i}(1/2)^{k+1}$ of that of the original image, i denotes the current iteration step number.
(c) The resized image is used as the new input image; then go to step 1. The iterative ROI selection algorithm can be terminated if the results of two consecutive iterations are close enough or by limiting the maximum number of iterations.

The output of the iterative ROI selection algorithm is denoted as $\boldsymbol{I}_{ROI}$. The iterative ROI selection produces better results than the original spectral residual algorithm. The equation to calculate the new size of the input image for each iteration is determined based on the size of an ovary in the ultrasound image. Experimental results showed the size of the selected ROI is about 1/4 of that of the original ultrasound image, which is sufficiently large to contain the ovary. Inside the selected region of interest, local minima identified by the enhanced labeled watershed algorithm are candidates of real follicles.

2.2. Follicle identification based on object growing

It is apparent that in PCOS ultrasound images, real follicles are surrounded by the ovary boundary and local minima outside the ovary are separated from real follicles by the ovary boundary. Characteristics of the region that is inside the ovary but not follicles are different from those of the region outside the ovary. Based on these observations, regions in a PCOS ultrasound image can be generally classified into three classes as shown in Fig. 2. Class 1 represents follicles; class 2 represents the region those are inside the ovary but not follicles; class 3 is the region outside the ovary. These three classes exhibit varied characteristics.

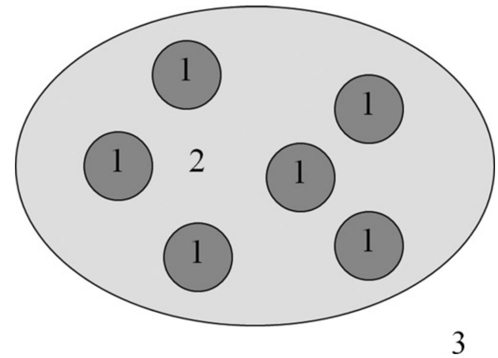

Fig. 2. Regions in a PCOS ultrasound image can be generally classified into three classes: class 1 represents follicles, class 2 represents the regions those are inside the ovary but not follicles, and class 3 is the region outside the ovary. These three classes exhibit different characteristics.

Follicles are local minima inside the ovary. Thus, if a convex hull [27] is constructed to include some local minima in the ovary, the convex hull should consist of regions of class 1 and class 2. Then if a new local minimum is included in the convex hull, there are two possibilities. One is that the new local minimum is inside the ovary. The new convex hull including the new local minimum should still consist of classes 1 and 2. The other possibility is that the new local minimum is outside the ovary and the resulting new convex hull should consist of all three classes.

With consideration of the ovary boundary, the differing characteristics of these three classes can be used to effectively determine the relationship of a local minimum with respect to the ovary boundary. In this section, we propose a method that is called follicle identification based on object growing. We first define an object cost function for the local minima based on a cost map, which represents the regional characteristics. Due to the process of the iterative ROI selection, local minima around the center of the region of interest can be assumed to be follicles with high probabilities and an initial set of follicles is formed by including these local minima. Then this initial set of follicles is expanded by adding new objects (other local minima) if their costs are less than a cost threshold that is dynamically computed and updated. The complete set of follicles can be found by gradually growing objects in the initial set. Although this process is similar to the region growing method [28], it should be noted that the region growing is based on pixels only while object growing is based on objects and thus takes into account the neighborhood information. The details of object growing are described as follows.

2.2.1. Object cost function

Assume that an image $\boldsymbol{I}$ has N objects of interest, labeled as 1, 2, ..., N, among which n objects (for the sake of simplicity, their labels are $1, 2, \ldots, n$) have been identified as elements of the target set T. We first construct the convex hull of the n objects and then define the cost of object i inside the convex hull of the n objects as follows.

$$Cost_{\text{internal}} = \frac{\sum_{(x,y)\in\Omega_{\text{int}}} C(x,y)}{\left|\Omega_{\text{int}}\right|}, \tag{9}$$

where C is the cost map representing properties of different regions in the image $\boldsymbol{I}$, which will be discussed in the next section, and the operator $|\Omega_{int}|$ denotes the cardinality of the set Ω_{int}, which is defined as

$$\Omega_{\text{int}} = \left\{ (x,y) \in G\Big(\bigcup_j S_j\Big) \cap G\Big(\overline{\bigcup_k S_k}\Big), \quad j=1,2,\ldots,n; \quad k=1,2,\ldots,n, \quad k \neq i \right\}, \tag{10}$$

where $\{S_1, S_2, \ldots, S_N\}$ is the set of regions occupied by the N objects in the image $\boldsymbol{I}$ and $G(\cdot)$ is a functionthat calculates the convex hull.

To understand the definition (10) better, define $A = G(\bigcup_j S_j)$, $j = 1, 2, \ldots, n$, and $B = \overline{G(\bigcup_k S_k)}$, $k = 1, 2, \ldots, n$, $k \neq i$. It can be seen that A is the convex hull containing n objects while B is the complement of the convex hull containing $n-1$ objects excluding object i. Thus, Ω_{int}, which is the intersection between A and B, represents the region induced by adding object i to the target set T.

Similarly, we define the cost of an object i' outside the convex hull of the n objects in the target set T as

$$Cost_{external} = \frac{\sum_{(x,y)\in\Omega_{ext}} C(x, y)}{\left|\Omega_{ext}\right|}, \tag{11}$$

where C is the same as that in Eq. (10) and the set Ω_{ext} is defined as

$$\Omega_{ext} = \left\{ (x, y) \in G(\bigcup_j S_j) \cap \overline{G(\bigcup_k S_k)},\quad j = 1, 2, \ldots, n, i';\quad k = 1, 2, \ldots, n \right\}. \tag{12}$$

Similarly, the set Ω_{ext} represents the region induced by adding object i' to the target set T. Finally, we define a cost threshold C_T as

$$C_T = \beta \cdot \frac{\sum_{(x,y)\in\Psi} C(x, y)}{\left|\Psi\right|}, \tag{13}$$

where β is a tuning parameter to be determined empirically and the set Ψ is defined as

$$\Psi = \left\{ (x, y) \in G(\bigcup_j S_j) \cap \overline{\bigcup_k S_k},\quad j = 1, 2, \ldots, n;\quad k = 1, 2, \ldots, n \right\}. \tag{14}$$

The set Ψ represents the region the convex hull of the n objects but excluding the n objects themselves. The cost threshold C_T is used as a criterion to add a new object or remove an existing object from the target set T. The parameter β represents the difference in the costs of the internal region and external region with respect to the ovary. A β value greater than 1 will ensure an initial set of follicles will grow as a result of the object growing algorithm, which is to be discussed later. The selection of β value will be further discussed in Section 3.

The example in Fig. 3 illustrates the sets Ω_{int}, Ω_{ext}, and Ψ defined above. Objects labeled as a, b, c, d, e, f and g represent candidates of follicles. It is further assumed that b, c, d, e, f and g are in the target set T. Then the set Ω_{int} for object g consists of pixels in the region C. The set Ω_{ext} for object a consists of pixels in the region A. Finally the set Ψ consists of pixels in the regions B and C excluding follicles.

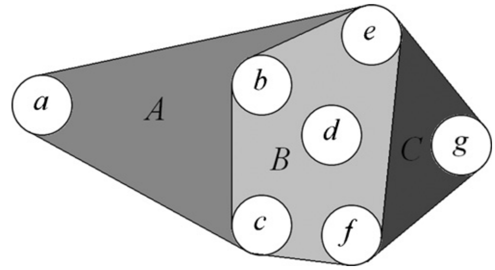

Fig. 3. The sets defined for computation of object cost functions. Assume that the objects b, c, d, e, f, and g are in the target set T. The set Ω_{int} for object g consists of pixels in the region C. The set Ω_{ext} for object a consists of pixels in the region A. Finally the set Ψ consists of pixels in the regions B and C (excluding the follicles).

2.2.2. Cost map

The object cost function defined in the previous section made use of the cost map $C(x,y)$, a function defined for each pixel (x,y)in the image. In order to detect follicles that are inside the ovary, the cost map should have different values depending on the pixel's relative location with respect to the ovary boundary. More specifically, pixels inside the ovary should have lower costs than their counterparts outside the ovary. In this paper, we define the cost map as a concatenation of three factors as follows.

$$C = \boldsymbol{I}_{ROI\_edge} \cdot \boldsymbol{I}_{ROI\_ovary\_mask} \cdot \boldsymbol{I}_{ROI\_mean}, \tag{15}$$

where three factors $\boldsymbol{I}_{ROI\_edge}$, $\boldsymbol{I}_{ROI\_ovary\_mask}$ and $\boldsymbol{I}_{ROI\_mean}$ represent different features of the image. First, $\boldsymbol{I}_{ROI\_edge}$ is obtained by applying Sobel edge detection to the region of interest $\boldsymbol{I}_{ROI}$ extracted in Section 2.1.3. $\boldsymbol{I}_{ROI\_edge}$ contains edge information for all the features in $\boldsymbol{I}_{ROI}$, including the ovary boundary, the local minima inside the ovary (corresponding to follicles), and the local minima outside the ovary. The edges of local minima in $\boldsymbol{I}_{ROI\_edge}$ should be further removed because they interfere with the effect of ovary boundary. The factor $\boldsymbol{I}_{ROI\_ovary\_mask}$ is defined for such purpose, which is obtained by dilating the mask $\boldsymbol{I}_{ROI\_min\_mask}$ with a 3×3 structuring element, where $\boldsymbol{I}_{ROI\_min\_mask}$ is a binary mask representing local minima. Finally, the factor $\boldsymbol{I}_{ROI\_mean}$ is the result of filtering $\boldsymbol{I}_{ROI}$ with a mean filter of size 3×3. The inclusion of $\boldsymbol{I}_{ROI\_mean}$ is based on the fact that pixels outside the ovary often have higher intensity values than those inside the ovary; thus the average of pixel values can effectively differentiate regions internal and external to the ovary. In summary, the computation of the cost map using these factors can effectively distinguish between regions internal and external to the ovary.

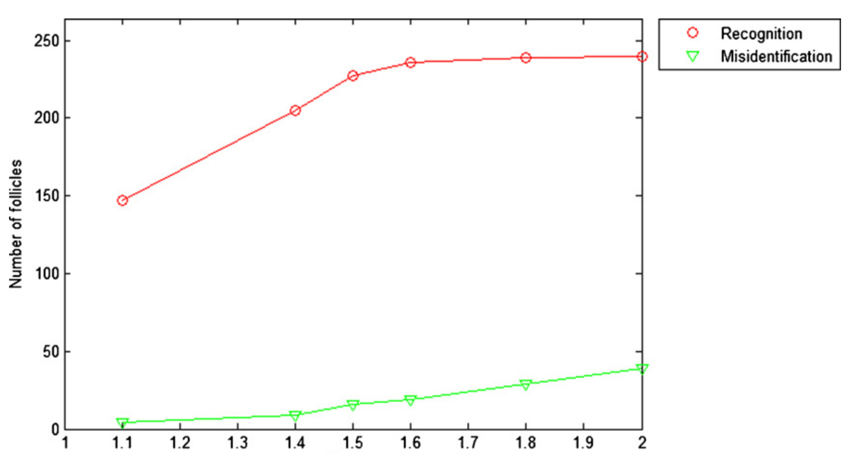

Fig. 4. The effects of β value on the recognized and misidentified follicles.

Table 1
Results of the proposed diagnostic system when the β changes.

Evaluation parameter	Results with different values of the β					
	β = 1.1	β = 1.4	β = 1.5	β = 1.6	β = 1.8	β = 2.0
Recognition rate	55.7%	77.6%	86.0%	89.4%	90.5%	90.9%
Misidentification rate	2.65%	4.21%	6.58%	7.45%	10.8%	14.0%
F_1 score	0.709	0.857	0.896	0.910	0.898	0.884

2.2.3. Object growing algorithm

With the object cost defined in previous sections, detailed steps of the object growing algorithm for follicle identification are described as follows.

(1) Find three objects (local minima) around the center of the region of interest and include them in the target set T. Initialize the cost threshold C_T according to (13) and the parameter β to a reasonable value (to be discussed in Section 3).
(2) Compute the convex hull for the elements of the set T. Calculate the cost of objects outside the convex hull according to (11). If the costs of some objects are less than or equal to the cost threshold C_T, add the one with the minimum cost to the set T.
(3) If any object is added to the set T, recalculate the cost threshold C_T and go to step 2. Otherwise go to step 4.
(4) Calculate the cost of each object inside the convex hull according to (9). Remove the objects whose costs are greater than the cost threshold C_T from the set T.

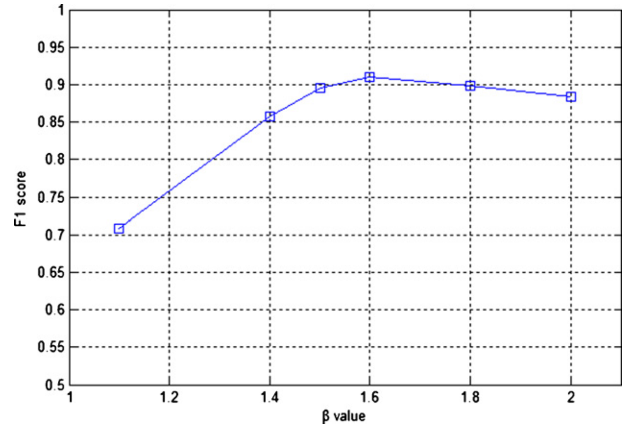

Fig. 5. F_1 scores of the proposed system with different values of β.

(5) If any object is removed from the set T, recalculate C_T and go to step 2. Otherwise stop. Record elements in the set T, which are the detected follicles found by the object growing algorithm.

From the object cost definition and the detailed steps described above, it can be seen that the object growing algorithm considers both the connectivity between objects and the neighborhood around them. The effectiveness of the object growing algorithm will be demonstrated by the experimental results to be discussed next.

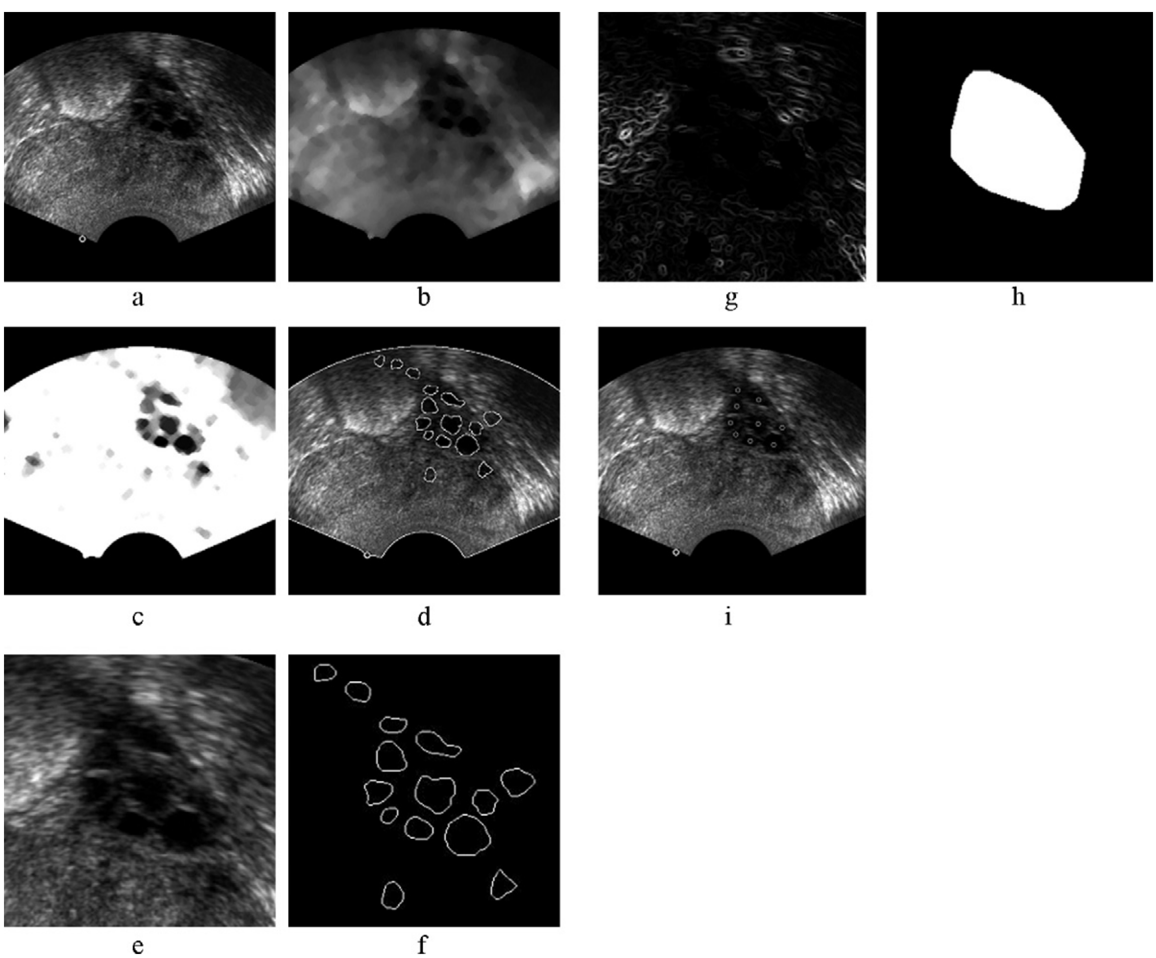

Fig. 6. The results of the proposed PCOS diagnostic system. (a) The original ultrasound ovary image. (b) Result of adaptive morphological filtering. (c) The gray depth image. (d) Result of the enhanced labeled watershed algorithm. (e) The selected region of interest. (f) Extracted candidates of follicles. (g) Cost map. (h) Result of the object growing algorithm. (i) Final result with circles indicating detected follicles.

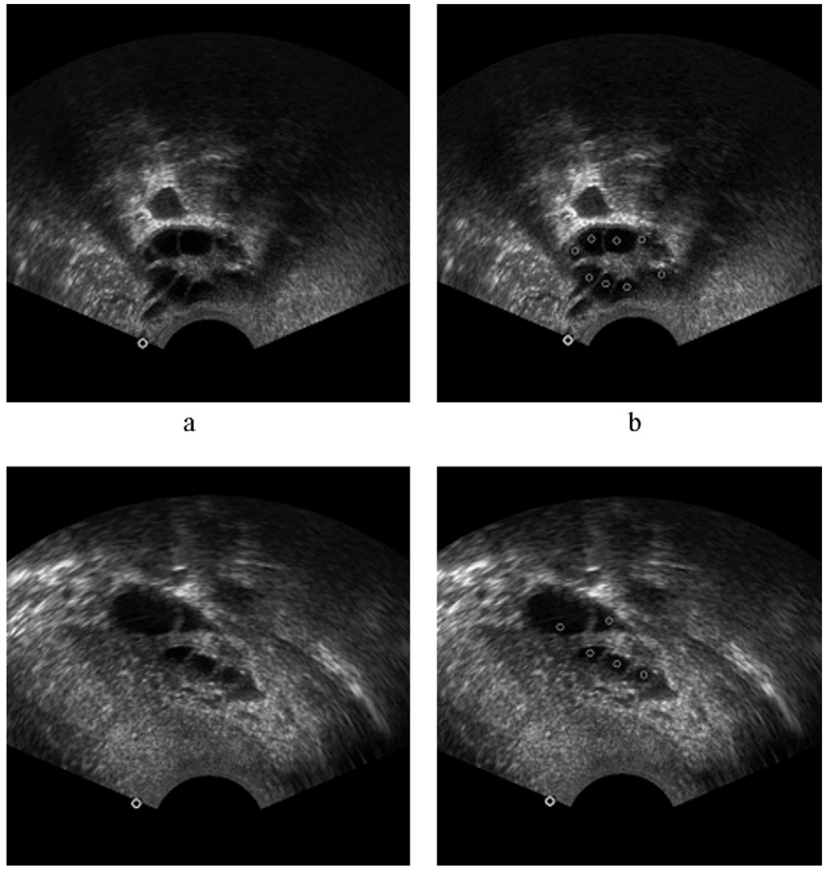

Fig. 7. Two ovary ultrasound images (a) and (c) and results of the proposed system (b) and (d), circles denote detected follicles.

3. Experimental results

Thirty-one ultrasound images were collected from PCOS patients with their consent using Philips Envisor 2540A Ultrasound System with a C8-4V trans-vaginal probe. All experiments are performed by Matlab 7.0 programs on a PC with Xeon CPU at 2.0 GHz and 2 GB memory. The execution time of the proposed method is around 30 s for processing an image. A total of 264 follicles were manually diagnosed by experienced physicians (gynecologists). To evaluate the effectiveness of follicle identification algorithms, two metrics are calculated: recognition rate (RR) and misidentification rate (MR). The recognition rate is defined as the ratio between recognized follicles (true positives) and all follicles (true positives and false negatives) while the misidentification rate is the ratio between all misidentified objects (false positives) and all recognized objects (true positives and false positives) [9–12].

As noted in Section 2, the tuning parameter β in the object growing algorithm denotes the cost difference of the internal region and external region with respect to the ovary. It represents the prior knowledge that the ovary is has relatively lower echo (or intensity) than other regions in the ultrasound image. Thus, when the initial target set contains objects that are inside the ovary, initializing β with a value greater than 1 ensures that the object growing algorithm will first expand the initial target set. Fig. 4 shows the effect of β value on the numbers of recognized and misidentified follicles. It can be seen both numbers monotonically increase when β increases. Table 1 shows the different RRs and MRs of the proposed diagnostic system when β changes and both RR and MR increase when β increases. To further investigate the effects of β value on the proposed algorithm, Fig. 5 plots the curve of F_1 score, which is an effective measure to simultaneously evaluate the RR and MR [29] and can be defined as

$$F_1 = 2 \cdot \frac{RR \cdot (1 - MR)}{RR + (1 - MR)} \tag{16}$$

A large value of F_1 score is desirable when F_1 score varies between 0 and 1. According to our experiments, β values greater than 1.5 produced acceptable results. In this paper, β is set to a fixed value of 1.6 in the proposed diagnostic system.

Fig. 6 shows the detailed results of the proposed diagnostic system applied to an ovary ultrasound image. Fig. 6(a) is the original image. Fig. 6(b) is the result of the adaptive morphological filtering and it can be seen that the speckle noise has been removed. Fig. 6(c) shows the gray depth image produced by equation (8). Fig. 6(d) shows the result of the enhanced labeled watershed algorithm. Fig. 6(e) shows the selected region of interest. Fig. 6(f) shows extracted candidates of follicles for the object growing algorithm. Fig. 6(g) shows the established cost map. Fig. 6(h) is the result of the object growing algorithm. Circles in Fig. 6(i) represent the detected follicles. It can be seen that the proposed diagnostic system is able to identify follicles accurately. Fig. 7 shows two more examples, in which the proposed method produced correct results.

To further demonstrate the effectiveness of the proposed algorithm, its performance is compared with three other proposed methods for follicle identification: geometric active contour using level set [15], boundary vector field (BVF) parametric active contour [14], and an FSVM classifier [16]. Both the level set based geometric active contour and the BVF parametric active contour are variants of the active contour model, which is a general method used to

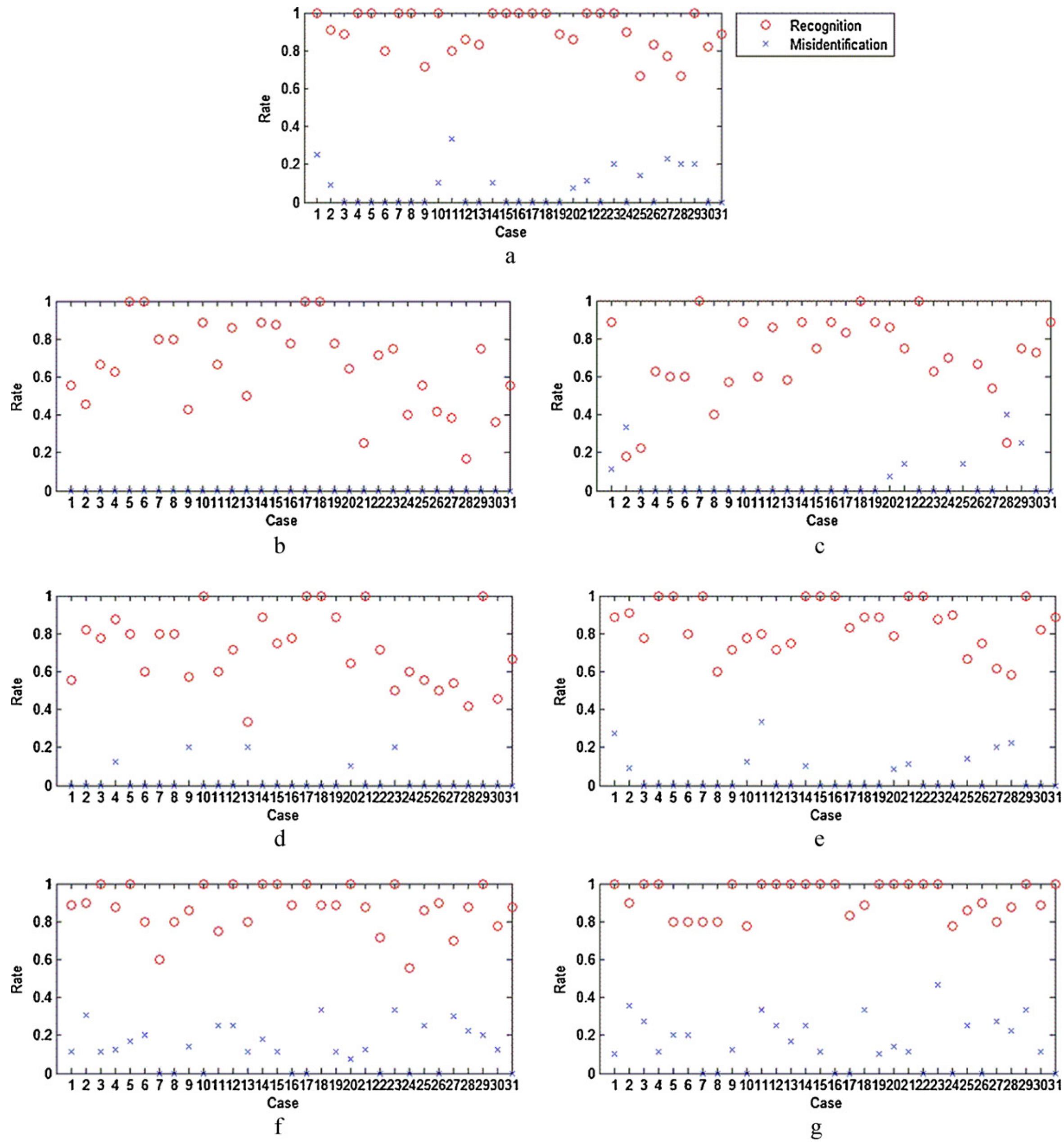

Fig. 8. Experimental results of different methods on 31 cases. (a) The proposed diagnostic system. (b) The level set method with circle initialization. (c) The level set method initialized with the object growing result. (d) The BVF method with circle initialization. (e) The BVF method initialized with the object growing result. (f) The FSVM classifier for the region of interest without PCA. (g) The FSVM classifier for the region of interest with PCA.

extract the object contour [30–33]. Both methods extract the ovary contour for the purpose of follicle identification. Results of the preprocessing phase of the proposed diagnostic system are used as inputs to both methods. Two initial contours are provided to both methods: one is a circle in the center of the region of interest and the other is the contour of the convex hull of objects computed by the object growing algorithm. The FSVM classifier is used to identify real follicles based on several features extracted for candidates of real follicles. A total of 18 features are computed for each follicle, which are the Roundness Criterion [34], mean value of saliency, mean distance to the center of the input image, and 15 coefficients extracted by the contourlet transform [35]. A total of 296 samples are obtained in the region of interest, which is selected by the preprocessing phase of the proposed system. The leaving-one method is used for this scheme.

Fig. 8 gives experimental results of 31 cases. Table 2 shows statistical results. The F_1 scores denote that the proposed diagnostic system is more effective than the other three methods. The RR of the proposed diagnostic system is 24.1% higher than the level set method and 13.1% higher than the BVF method on average. It could also be observed that the level set method and the BVF method achieve relatively lower MRs compared with that of the proposed method. The reason is mainly that these two methods just tend to converge on the more primary local minima. So the MR could be relatively lower but the RR would be lower at the same time. It results in the degradation of the entire performance of the diagnostic system compared with the proposed method. From Table 2, it can also be seen that using the result of the proposed object growing algorithm to initialize the BVF method produced relatively better results, demonstrating the effectiveness of the proposed diagnos-

Table 2
Comparison of the proposed diagnostic system and other methods.

Methods		Results		
		Recognition rate	Misidentification rate	F_1 score
The proposed diagnostic system (β = 1.6)		89.4%	7.45%	0.910
Level set	Circle initialization	61.7%	0.00%	0.763
	Initialization of object growing's result	68.9%	4.21%	0.801
BVF	Circle initialization	68.9%	2.67%	0.807
	Initialization of object growing's result	83.3%	6.38%	0.882
FSVM classifier	No PCA compression	81.5%	14.9%	0.833
	PCA compression	86.5%	17.6%	0.844

tic system. The RR and MR of the FSVM classifier method are 81.5% and 14.9%. The PCA method [36] was also used in the FSVM classifier to reduce the dimensionality, which produced RR and MR of 86.5% and 17.6%, respectively. However it is worth to note that the performance of the FSVM classifier dropped significantly without using the results of the preprocessing phase in the proposed diagnostic system as inputs. In our experiments, the RR and MR of the FSVM classifier dropped to 69.5% and 29.5%, and 73.5% and 26.5% with the use of PCA.

Results of other automatic systems recently published are reported as 88% RR and 36% MR for [9], 78% RR and 29% MR for [10,11], and 60% RR and 30% MR for [12]. It can be seen that the proposed diagnostic system is more effective with 89.4% RR and 7.45% MR.

4. Discussions

As human visual system is extraordinarily competent, the proposed object growing algorithm for follicle identification was inspired by the cognitive process of the human visual system [37]. It was reported that human perceptual performance of objects is based on their prior knowledge. Accurate object recognition needs the knowledge of how the correct result is formed through the prior knowledge [37]. For follicle identification, experienced physicians first locate possible follicles that are low echo regions with relatively regular shapes. Then with such prior knowledge they search the most possible contour of the ovary. The search criterion is that the contour should contain converged possible follicles and the internal region of the contour should be homogeneous. At the same time the contour should be coincident with the inconspicuous boundary of the ovary in the ultrasound image. The search process by experienced physicians is dynamic and accomplished in a very short time. Finally they accurately recognize all the follicles inside the ovary.

The proposed object growing for follicle identification is an artificial intelligent method that well mimics the cognitive process of medical experts and simultaneously considers the properties of follicles, the different region information in the ovary ultrasound image and the boundary information of the ovary. In this algorithm, objects are basic elements, which emphasize the effect of the prior knowledge. Objects used as follicle candidates are searched with features that one real follicle should have. This treatment ensures that properties of follicles are introduced in the algorithm. Then the cost map is established to distinguish between regions internal and external to the ovary. Based on the cost map, the convex hull of possible follicles is used to search the most possible set of objects as follicles. This process emphasizes the spatial connectivity of follicles and the contour of the ovary which contains follicles. The boundary information of the ovary is embedded in the iterative process. The dynamic minimization of the cost function and the initialization of the most possible follicle candidates ensure the convergence of the proposed method.

5. Conclusion

This paper proposed an automated system for diagnosis of polycystic ovary syndrome using ultrasound images. The proposed system consists of two major functional blocks: preprocessing phase and follicle identification based on object growing. In the preprocessing phase, the speckle noise in the input image is removed by an adaptive morphological filter, then contours of objects are extracted using an enhanced labeled watershed algorithm, and finally the region of interest is automatically selected. The object growing algorithm for follicle identification first computes a cost map to distinguish the ovary and its external region and assigns each object a cost function based on the cost map. The object growing algorithm initially selects several objects that are likely to be follicles with very high possibility and dynamically update the set of possible follicles based on their cost functions. The proposed automated diagnostic system was applied to 31 real PCOS ultrasound images and it achieved a recognition rate of 89.4%. The proposed method is more effective than three other methods discussed in this paper and other recently reported methods.

References

[1] Affiliates of Medifocus.com. Medifocus guidebook: polycystic ovary syndrome. Silver Spring: Medifocus.com, Inc.; 2007.
[2] Franks S. Polycystic ovary syndrome. Medicine 2005;33:38–40.
[3] Burckhardt CB. Speckle in ultrasound B-mode scans. IEEE Transactions on Sonics and Ultrasonics 1978;25:1–6.
[4] Loizou CP, Pattichis CS, Christodoulou CI, Istepanian RSH, Pantziaris M, Nicolaides A. Comparative evaluation of despeckle filtering in ultrasound imaging of the carotid artery. IEEE Transactions on Ultrasonics, Ferroelectrics and Frequency Control 2005;52:1653–69.
[5] Muzzolini R, Yang YH, Pierson R. Multiresolution texture segmentation with application to diagnostic ultrasound images. IEEE Transactions on Medical Imaging 1993;12:108–23.
[6] Pierson RA, Adams GP. Computer-assisted image analysis, diagnostic ultrasonography and ovulation induction: strange bedfellows. Theriogenology 1995;43:105–12.
[7] Sarty GE, Liang W, Sonka M, Pierson RA. Semiautomated segmentation of ovarian follicular ultrasound images using a knowledge based algorithm. Ultrasound in Medical Biology 1998;24:27–42.
[8] Krivanek A, Sonka M. Ovarian ultrasound image analysis: follicle segmentation. IEEE Transactions on Medical Imaging 1998;17:935–44.
[9] Potočnik B, Zazula D. Automated ovarian follicle segmentation using region growing. In: First international workshop on image and signal processing and analysis. 2000. p. 157–62.
[10] Potočnik B, Zazula D. Automated analysis of a sequence of ovarian ultrasound images. Part I: segmentation of single 2D images. Image and Vision Computing 2002;20:217–25.
[11] Potočnik B, Zazula D. Automated analysis of a sequence of ovarian ultrasound images. Part II: prediction-based object recognition from a sequence of images. Image and Vision Computing 2002;20:227–35.
[12] Cigale B, Zazula D. Segmentation of ovarian ultrasound images using cellular neural networks. International Journal of Pattern Recognition and Artificial Intelligence 2004;18:563–81.
[13] Tao Z, Tagare HD. Tunneling descent for m.a.p. active contours in ultrasound segmentation. Medical Image Analysis 2007;11:266–81.
[14] Sum KW, Cheung PYS. Boundary vector field for parametric active contours. Pattern Recognition 2007;40:1635–45.

[15] Yang XS, Wang YY, Wang Y, Wang Y. Boundary extraction of ultrasonic breast tumor image based on improved variational level set methods. Space Medicine & Medical Engineering 2008;12:500–4.
[16] Jiang XF, Yi Z, Lv JC. Fuzzy SVM with a new membership function. Neural Computing & Applications 2006;15:268–76.
[17] Man ZH, Wu HR, Liu S, Yu XH. A new adaptive backpropagation algorithm based on Lyapunov stability theory for Neural Networks. IEEE Transactions on Neural Networks 2006;17:1580–91.
[18] Deng YH, Wang YY, Wang WQ. Medical ultrasound image denoising based on adaptive morphological despeckling filter. Opto-Electronic Engineering 2008;35:115–21.
[19] Hou XD, Zhang LQ. Saliency detection: a spectral residual approach. Computer Vision and Pattern Recognition 2007:1–8.
[20] Yu Y, Acton ST. Speckle reducing anisotropic diffusion. IEEE Transactions on Image Processing 2002;11:1260–70.
[21] Aysal TC, Barner KE. Rayleigh-maximum-likelihood filtering for speckle reduction of ultrasound images. IEEE Transactions on Medical Imaging 2007;5:712–27.
[22] Rabbani H, Vafadust M, Abolmaesumi P, Gazor S. Speckle noise reduction of medical ultrasound images in complex wavelet domain using mixture priors. IEEE Transactions on Biomedical Engineering 2008;9:2152–60.
[23] Gonzalez RC, Woods RE. Digital image processing. New Jersey: Prentice Hall Inc.; 2002.
[24] Beucher S, Meyer F. The morphological approach of segmentation: the watershed transformation. In: Dougherty E, editor. Mathematical morphology in image processing. New York: Marcel Dekker; 1992.
[25] Itti L, Koch C. A saliency-based search mechanism for overt and covert shifts of visual attention. Vision Research 2000;10:1489–506.
[26] Wolfe J, Oliva A, Horowitz T, Butcher S, Bompas A. Segmentation of objects from backgrounds in visual search tasks. Vision Research 2002;28:2985–3004.
[27] Barber CB, Dobkin DP, Huhdanpaa HT. The quickhull algorithm for convex hulls. ACM Transactions on Mathematical Software 1996;22:469–83.
[28] Hojjatoleslami SA, Kittler J. Region growing: a new method. IEEE Transactions on Image Processing 1998;7:1079–84.
[29] Van Rijsbergen CJ. Information retrieval. Newton, MA: Butterworth-Heinemann; 1979.
[30] Kass M, Witkin A, Terzopoulos D. Snakes: active contour models. Computer Vision 1988;1:321–31.
[31] Osher S, Sethian J. Fronts propagating with curvature-dependent speed: algorithms based on Hamilton–Jacobi formulations. Computational Physics 1988;79:12–49.
[32] Zimmer C, Olivo-Marin JC. Coupled parametric active contours. IEEE Transactions on Pattern Analysis and Machine Intelligence 2005;27:1838–42.
[33] Chan T, Vese L. Active contours without edges. IEEE Transactions on Image Processing 2001;10:266–77.
[34] Deng YH, Wang YY, Chen P. Automated detection of polycystic ovary syndrome from ultrasound images. In: IEEE EMBS conference. 2008. p. 4772–5.
[35] Do MN, Vetterli M. The contourlet transform: an efficient directional multiresolution image representation. IEEE Transactions on Image Processing 2005;14:2091–106.
[36] Szu H, Zhang LM. Intelligent visual image processing. Shanghai: Shanghai Science and Technology Education Press; 2002.
[37] Kersten D, Mamassian P, Yuille AL. Object perception as bayesian inference. Annual Review of Psychology 2004;55:271–304.